

赵令浩, 孙冬阳, 胡明月, 等. 激光剥蚀-扇形磁场电感耦合等离子体质谱法同时测定锆石 U-Pb 年龄和微量元素含量[J]. 岩矿测试, 2024, 43(1): 47–62. DOI: 10.15898/j.ykcs.202309110151.

ZHAO Linghao, SUN Dongyang, HU Mingyue, et al. Simultaneous Determination of U-Pb Age and Trace Elements of Zircon by Laser Ablation Sector Field Inductively Coupled Plasma-Mass Spectrometry[J]. Rock and Mineral Analysis, 2024, 43(1): 47–62. DOI: 10.15898/j.ykcs.202309110151.

激光剥蚀-扇形磁场电感耦合等离子体质谱法同时测定锆石 U-Pb 年龄和微量元素含量

赵令浩, 孙冬阳, 胡明月, 袁继海, 范晨子, 詹秀春

(中国地质调查局元素微区与形态分析重点实验室, 国家地质实验测试中心, 北京 100037)

摘要: 激光剥蚀-扇形磁场电感耦合等离子体质谱 (LA-SF-ICP-MS) 具有高灵敏度特征, 被广泛应用于锆石等含 U 矿物原位微区 U-Pb 定年研究, 但磁偏转式质量分析器的使用导致该质谱仪扫描速度相对较慢, 可能影响 U-Pb 同位素与其他关键微量元素的同时采集。本文通过优化仪器信号稳定性和实验方法, 对目前常用的 7 种锆石 U-Pb 标准样品进行 U-Pb 定年和 Ti、REEs、Hf 等关键元素同时定量分析, 探讨了多元素同时分析方法的可行性及对于 U-Pb 定年结果的影响。实验结果表明, 相对于 LA-SF-ICP-MS 仅检测 U-Pb 同位素方法, 同时开展多元素含量检测可能会使 U-Pb 同位素信号强度稳定性下降, 导致单点 U-Pb 年龄结果误差及离散程度增大。与仅测定 U-Pb 同位素年龄的测定结果相比较, 根据不同锆石样品中 U-Pb 同位素含量高低, 多元素同时检测获得分析点的 $^{206}\text{Pb}/^{238}\text{U}$ 年龄和 $^{207}\text{Pb}/^{235}\text{U}$ 年龄变化范围不同程度地增大, 其中 $^{207}\text{Pb}/^{235}\text{U}$ 年龄受影响明显, 单点 $^{207}\text{Pb}/^{235}\text{U}$ 年龄误差从 ~1.5% 增大至 ~2.0%, 单点年龄的相对标准偏差 (RSD) 从 0.5%~1.3% 增大至 1.2%~3.3%。尽管如此, 多元素同时检测方法对于各样品最终测定年龄没有明显的影响, 相对于 TIMS 年龄, 各样品的谐和年龄和 $^{206}\text{Pb}/^{238}\text{U}$ 加权平均年龄偏差分别小于 1.0% 和 0.7%, 完全满足 U-Pb 同位素地质年代学测试要求。同时测定锆石样品中的关键微量元素含与其推荐值相对误差小于 10%。因此, 采用 LA-SF-ICP-MS 可以同时准确地测定锆石 U-Pb 年龄和微量元素含量, 该方法亦可用于其他副矿物 U-Pb 年龄与关键微量元素同时测定。

关键词: 激光剥蚀-扇形磁场电感耦合等离子体质谱 (LA-SF-ICP-MS); 锆石; U-Pb 定年; 微量元素
要点:

- (1) LA-SF-ICP-MS 同时测定锆石 U-Pb 和多种微量元素含量时, U-Pb 同位素信号和比值的稳定性会受到影响, 导致单分析点 U-Pb 定年结果不确定度增大, 但对样品谐和年龄(基于多分析点统计计算结果)准确度没有影响, 精密度略有降低。
- (2) LA-SF-ICP-MS 同时测定锆石 U-Pb 年龄和微量元素含量, 获得锆石 U-Pb 年龄偏差小于 1%, REEs、Ti、Hf、Pb、Th 和 U 等关键微量元素含量偏差小于 10%, 满足高精度 U-Pb 定年分析需求。
- (3) LA-SF-ICP-MS 仅测定锆石 U-Pb 年龄可以有效地降低单点同位素比值测试引入的误差, 获得高精密度 ($2\sigma < 2\%$) 和高准确度 ($\text{RSE} < 0.5\%$) 定年结果。

中图分类号: P597.3; O657.63

文献标识码: A

锆石、榍石、磷灰石、独居石等副矿物在地质样品中广泛存在, 这些矿物普遍铀含量较高, 因此成为

U-Pb 定年的目标矿物^[1-5]。同时相对于普通造岩矿物, 副矿物是各种关键微量元素如 Zr、Hf、P、Ti、

收稿日期: 2023-09-11; 修回日期: 2024-01-02; 接受日期: 2024-01-15

基金项目: 国家重点研发计划项目 (2021YFC2903101); 中国地质科学院基本科研业务费项目 (CSJ202201)

作者简介: 赵令浩, 博士, 副研究员, 从事地球化学及构造地质学研究。E-mail: linghaozhao@126.com。

Nb、Ta、稀土元素(REEs)、U、Th等的主要载体,通过副矿物微量元素特征可以为划分年龄期次、解译年龄意义提供参考。例如,利用锆石Th/U比值及REEs配分模式特征区分岩浆及变质成因锆石^[6-8];根据独居石中Y含量区分其与石榴子石或磷钇矿共生^[9];根据碎屑磷灰石中微量元素含量区分磷灰石成因及来源,进而实现磷灰石U-Pb年龄溯源统计^[10-11];另一方面副矿物微量元素含量可以提供矿物形成温度、氧逸度等信息,例如锆石Ti温度计^[12]、榍石Zr温度计^[13]、Ce氧逸度等^[14]。变质或部分熔融过程中,副矿物的参与可能对岩石与流体系统的关键微量元素或同位素体系产生明显的影响^[15-19],结合现代地质体中副矿物U-Pb年龄、关键微量元素特征及同位素特征构建变质矿物P-T-t轨迹,反演矿物生长过程,是“岩石年代学(Petrochronology)”研究中的重要组成部分^[20]。因此,采用微区分析技术在有限的分析空间内获得更多的元素或同位素信息至关重要。

LA-ICP-MS技术因其高效、准确的特征成为副矿物U-Pb定年的主要技术方法之一,近年来随着含普通铅副矿物U-Pb定年数据处理方法不断完善和仪器测试能力的提高,U-Pb定年目标矿物领域不断拓展,尤其低/超低U矿物U-Pb定年方法的建立为解决传统疑难地质问题提供有力的技术支撑^[21-25]。

根据质谱接收系统差异,激光剥蚀与多接收质谱联用构成LA-MC-ICP-MS,该仪器具有高灵敏度特征,可以同时采集数种元素或同位素信号,用于同位素比值的准确测定,但无法进行微量元素定量分析。为实现原位U-Pb同位素定年和微量元素含量同时检测,Kylander-Clark等(2013)^[26]提出采用多接收质谱和单接收质谱串联(LASS)设计,分别用于U-Pb定年和微量元素定量分析。

激光剥蚀与单接收质谱连接构成LA-ICP-MS,尽管只有一个检测器,但可实现大范围质量数元素/同位素快速顺序检测,目前多用于微区微量元素定量分析和副矿物U-Pb同位素定年。单接收质谱根据质量分析器差异又可分为四极杆质谱(Q-ICP-MS)和扇形磁场质谱(SF-ICP-MS),Hattendorf等(2003)^[27]详细对比了两种质谱结构和性能的差异。总体上,Q-ICP-MS顺序扫描速度较快(2~50Hz),但灵敏度相对较低,广泛应用于锆石、榍石、磷灰石等相对高U、Pb矿物U-Pb年龄与关键微量元素含量同时分析。SF-ICP-MS具有高灵敏度、高分辨率特征,其灵敏度可达1000~10000cps/(μg/g),根据副矿物中的U-Pb含量,扇形磁场质谱更利于高空间分辨

率和超低U含量样品的U-Pb定年分析。例如Kooijman(2012)^[28]采用LA-SF-ICP-MS实现了12μm锆石U-Pb定年;Wu等(2020)^[29]通过改造LA-SF-ICP-MS进样系统,大幅度提升了质谱仪的灵敏度,并且实现了高空间分辨率(5~16μm)锆石U-Pb定年。另外,SF-ICP-MS与激光系统联用实现了低/超低U矿物U-Pb定年,例如对U含量在ng/g级的碳酸盐矿物进行准确的U-Pb定年等^[23,30]。但是受限于磁场定位时间较长,扫描速度较慢,根据选择分析元素质量范围,典型扫描速度1~5Hz,远低于Q-ICP-MS。尽管Latkoczy等(2002)^[31]采用LA-SF-ICP-MS准确测定了样品中多元素含量,并提出通过优化设置可以使分析不受质谱扫描速度的影响,但相对于元素定量分析,尤其是在相对较少数据统计量的情况下,同位素比值的测定对于仪器准确性和稳定性提出更高的要求。为保证年龄结果的准确性与稳定性,目前报道的采用高分辨质谱(SF-ICP-MS)测定副矿物U-Pb年龄方法中一般仅测试与U-Pb年龄相关的同位素(²⁰²Hg~²³⁸U),无法同时进行关键微量元素定量分析。在多期次生长副矿物研究中,U-Pb年龄与微量元素含量分别测试一方面可能会受到矿物生长空间影响,不便开展多次取样;另一方面非原位测试可能会导致测定年龄与微量元素所反映的温度、压力等地质环境信息耦合困难。

基于锆石U-Pb定年与微量元素含量同时测定在“岩石年代学”领域的重要性,本文采用激光剥蚀扇形磁场等离子体质谱(LA-SF-ICP-MS),以25μm激光斑束对7种常见的锆石U-Pb标准样品,包括91500^[32]、GJ-1^[33]、Tanz^[34]、SA01^[35]、Temora1^[36]、Plešovice^[37]和Qinghu^[38]进行U-Pb年龄和Ti、Hf、REEs等关键元素含量的同时定量分析,探讨LA-SF-ICP-MS同时进行U-Pb定年和微量元素定量分析方法的可行性及其对年龄结果的影响。

1 实验部分

1.1 锆石U-Pb样品及处理

实验中采用的锆石U-Pb样品按其年龄由高到低包括:91500^[32]、GJ-1^[33]、Tanz^[34]、SA01^[35]、Temora1^[36]、Plešovice^[37]和Qinghu^[38],年龄范围为1064~159Ma。这些矿物样品具有稳定的ID-TIMS U-Pb年龄,在世界范围内被广泛用作U-Pb定年标准样品。本文通过分析这些样品以验证所建立测试方法的准确性。

91500锆石是应用最为广泛的锆石U-Pb定年标准样品。该样品的ID-TIMS $^{206}\text{Pb}/^{238}\text{U}$ 年龄为1062Ma^[32]。GJ-1锆石是澳大利亚MacQuarie大学大陆地球化学与成矿作用研究中心实验室的U-Pb测定标准锆石^[33]。该锆石的TIMS年龄结果不谐和, $^{206}\text{Pb}/^{238}\text{U}$ 和 $^{207}\text{Pb}/^{235}\text{U}$ 年龄分别为 $599.8 \pm 1.7\text{ Ma}$ 和 $601.6 \pm 1.3\text{ Ma}$,但是LA-ICP-MS分析结果谐和,目前该样品LA-ICP-MS分析中采用参考年龄为~603Ma。Tanz锆石是中国地质大学(武汉)团队开发的锆石U-Pb定年和Zr-O同位素组成标准样品。该样品的ID-TIMS年龄为 $566.16 \pm 0.77\text{ Ma}$, SIMS和LA-ICP-MS分析结果都介于 $564 \sim 569\text{ Ma}$,表明该样品具有良好的U-Pb同位素均一性^[34]。SA01锆石是中国科学院地质与地球物理研究所近年来开发的锆石U-Pb定年、Hf-O同位素组成微区测试标准物质。该样品的ID-TIMS年龄为 $535.1 \pm 0.3\text{ Ma}$ ^[35]。Temora1锆石产自澳大利亚Lachlan造山带镁铁质岩,目前常用作SHRIMP锆石U-Pb定年标准样品。该样品的ID-TIMS年龄为 $416.75 \pm 0.24\text{ Ma}$ ^[36]。Plešovice锆石产自捷克富钾麻粒岩,该样品ID-TIMS测定的 $^{206}\text{Pb}/^{238}\text{U}$ 年龄为 $337.13 \pm 0.37\text{ Ma}$ ^[37]。Qinghu锆石是中国科学院地质与地球物理研究所离子探针实验室标准锆石。该样品的TIMS谐和年龄为 $159.38 \pm 0.12\text{ Ma}$ ^[38]。

将所有锆石样品粘在PVC模具底部,然后向模具中注入环氧树脂和固化剂,制备成直径约24mm锆石靶,并对样品靶表面进行打磨、抛光,直至样品露出光洁表面。采用光学显微镜结合扫描电镜拍摄样品在透射光和放射光下照片及阴极发光(CL)图片,观察样品内部结构特征,避免样品裂隙及包裹体

等对测试结果造成影响。在激光剥蚀分析前,利用去离子水及无水乙醇擦拭锆石表面,并采用高压N₂流吹扫样品,去除样品表面的普通Pb污染。

1.2 仪器设置

锆石U-Pb定年和微量元素含量分析在中国地质调查局元素微区与形态分析重点实验室完成,采用ESLNWR193^{UC}ArF准分子激光器及ELEMENT II扇形磁场高分辨电感耦合等离子体质谱仪(SF-ICP-MS,美国ThermoFisher Scientific公司)。

本实验中激光剥蚀采用 $25\mu\text{m}$ 激光斑束,频率8Hz。以He气作为吹扫气体提高剥蚀气溶胶传输效率^[39],并通入1mL/min氮气以提高仪器灵敏度^[40]。气路上采用信号匀化装置,增大气溶胶扩散空间,可有效地提高样品剥蚀信号稳定性。

SF-ICP-MS分析采用低分辨模式($M/\Delta M=300$)。实验前采用 $25\mu\text{m}$ 激光线扫描NIST612进行仪器调谐,使La和Th信号 $>1.5 \times 10^5\text{ cps}$,信号稳定性(RSD)为1%~2%,同时监测 ThO^+/Th^+ 控制氧化物产率 $<0.2\%$ 。选择分析锆石U-Pb同位素和微量元素,包括 ^{29}Si 、 ^{49}Ti 、 ^{89}Y 、 ^{91}Zr 、 ^{139}La 、 ^{140}Ce 、 ^{141}Pr 、 ^{146}Nd 、 ^{147}Sm 、 ^{151}Eu 、 ^{157}Gd 、 ^{159}Tb 、 ^{163}Dy 、 ^{165}Ho 、 ^{166}Er 、 ^{169}Tm 、 ^{172}Yb 、 ^{175}Lu 、 ^{178}Hf 、 ^{206}Pb 、 ^{207}Pb 、 ^{208}Pb 、 ^{232}Th 和 ^{238}U ,该质量数范围内质谱磁场定位4次,设置首次磁场定位时间为0.1s,其余磁场定位时间0.05s。 ^{206}Pb 、 ^{208}Pb 、 ^{232}Th 和 ^{238}U 测试时间10ms, ^{207}Pb 测试时间20ms,其余各元素测试时间5ms,每次扫描总时间0.87s,有效分析时间占71%。多数锆石中不含或含极低普通铅,且采用单接收质谱难以准确测定 ^{204}Pb 用于普通铅校正,为提高有效分析时间的比例,本方法中未检测 ^{202}Hg 和 ^{204}Pb 。仪器工作条件见表1。

表1 LA-SF-ICP-MS仪器工作条件

Table 1 Working conditions for LA-SF-ICP-MS instrument.

激光剥蚀系统(NWR 193UC)		高分辨电感耦合等离子体质谱仪(Element II)	
实验参数	工作条件	实验参数	工作条件
波长	193nm	射频功率	1200W
脉冲时间	15ns	冷却气(Ar)流速	16L/min
激光斑束	25μm	辅助气(Ar)流速	0.9L/min
激光频率	8Hz	样品气(Ar)流速	0.82L/min
能量密度	~3.2J/cm ²	分辨率	低($M/\Delta M=300$)
载气流速(He)	0.8L/min	扫描模式	E-Scan ^{29}Si , ^{49}Ti , ^{89}Y , ^{91}Zr , ^{139}La , ^{140}Ce , ^{141}Pr , ^{146}Nd , ^{147}Sm , ^{151}Eu , ^{157}Gd , ^{159}Tb , ^{163}Dy , ^{165}Ho , ^{166}Er , ^{169}Tm , ^{172}Yb , ^{175}Lu , ^{178}Hf , ^{206}Pb , ^{207}Pb , ^{208}Pb , ^{232}Th , ^{238}U
增敏气流速(N ₂)	1mL/min	扫描质量	Both模式(Counting和Analog)
剥蚀时间	40s	接收器模式	

1.3 数据处理

LA-ICP-MS 测试前采用大激光斑束对样品表面进行预剥蚀, 去除样品表面可能存在的 Pb 同位素污染。样品分析采用点剥蚀模式, 点分析时间 90s, 包括仪器背景信号采集时间 20s, 激光剥蚀信号采集时间 40s, 以及吹扫时间 30s。

采用 91500 镐石和 NIST610 分别作为 U-Pb 同位素比值和微量元素定量分析的标准物质。每分析 10 个未知样品点插入分析一组标准样品(2 点 91500 镐石和 1 点 NIST610)以校正分馏效应。

镐石 U-Pb 年龄和微量元素含量数据处理采用 GLITTER 4.0 软件完成^[41], 选择标准样品传递误差 1%(Std Uncertainty), 所有样品与 91500 标准镐石截取相同信号区间。镐石年龄谐和图和加权平均图绘制采用 Isoplot^[42]。镐石微量元素含量计算分别以 Si(SiO₂ 含量 32.8%) 和 Zr(ZrO₂ 含量 67.2%) 作为内标。本文所有年龄值和同位素比值误差均为 2σ 。

2 结果与讨论

扇形磁场质谱(SF-ICP-MS)具有低背景、高灵敏度特征, 在镐石 U-Pb 定年过程中可以有效地提高空间分辨率和分析的准确度。因此, LA-SF-ICP-MS 在低 U-Pb 含量年轻镐石及其他低 U 矿物如石榴子石、方解石等矿物定年中有独特的优势。但由于 SF-ICP-MS 扫描多元素过程中磁场定位时间的影响, 当测量元素质量数大范围变化时, 其扫描速度明显降低, 因此采用 LA-SF-ICP-MS 测定镐石年龄时一般仅检测²⁰²Hg、²⁰⁴Pb、²⁰⁶Pb、²⁰⁷Pb、²⁰⁸Pb、²³²Th 和²³⁸U 等与 U-Pb 定年相关的 7 个同位素。本文中采用的方法在检测 U-Pb 相关同位素的基础上, 同时检测镐石中的关键主、微量元素含量, 包括 Si、Ti、REEs、Hf 等(表 1), 并对采集与未采集微量元素两种方法定年结果进行对比, 测试结果如图 1、图 2、表 2 和表 3 所示。

2.1 LA-SF-ICP-MS 镐石 U-Pb 定年和多元素含量同时分析方法定年结果

91500 镐石: 测试样品 30 点, 获得单点²⁰⁶Pb/²³⁸U 和²⁰⁷Pb/²³⁵U 年龄分别为 1045.7~1080.5Ma 和 1044.0~1093.0Ma, 单点误差分别为 20.3~22.7Ma(1.9%~2.1%) 和 14.1~21.7Ma(1.7%~2.0%)。在谐和图上所有样品点呈现谐和特征, 获得 U-Pb 谐和年龄 1063.3 ± 2.4 Ma(图 1a), ²⁰⁶Pb/²³⁸U 加权平均年龄为 1062.8 ± 7.3 Ma(图 1b), MSWD=0.24, 与推荐值在误差范围内一致。

— 50 —

GJ-1 镐石: 测试样品 37 点, 获得单点²⁰⁶Pb/²³⁸U 和²⁰⁷Pb/²³⁵U 年龄分别为 599.1~610.4Ma 和 563.4~618.3Ma, 单点误差分别为 11.4~12.4Ma (~1.9%) 和 9.8~12.7Ma(1.6%~2.1%)。该样品整体谐和年龄为 603.8 ± 1.6 Ma(图 1c), ²⁰⁶Pb/²³⁸U 加权平均年龄为 604.0 ± 3.8 Ma(图 1d), 与推荐年龄在误差范围内一致。

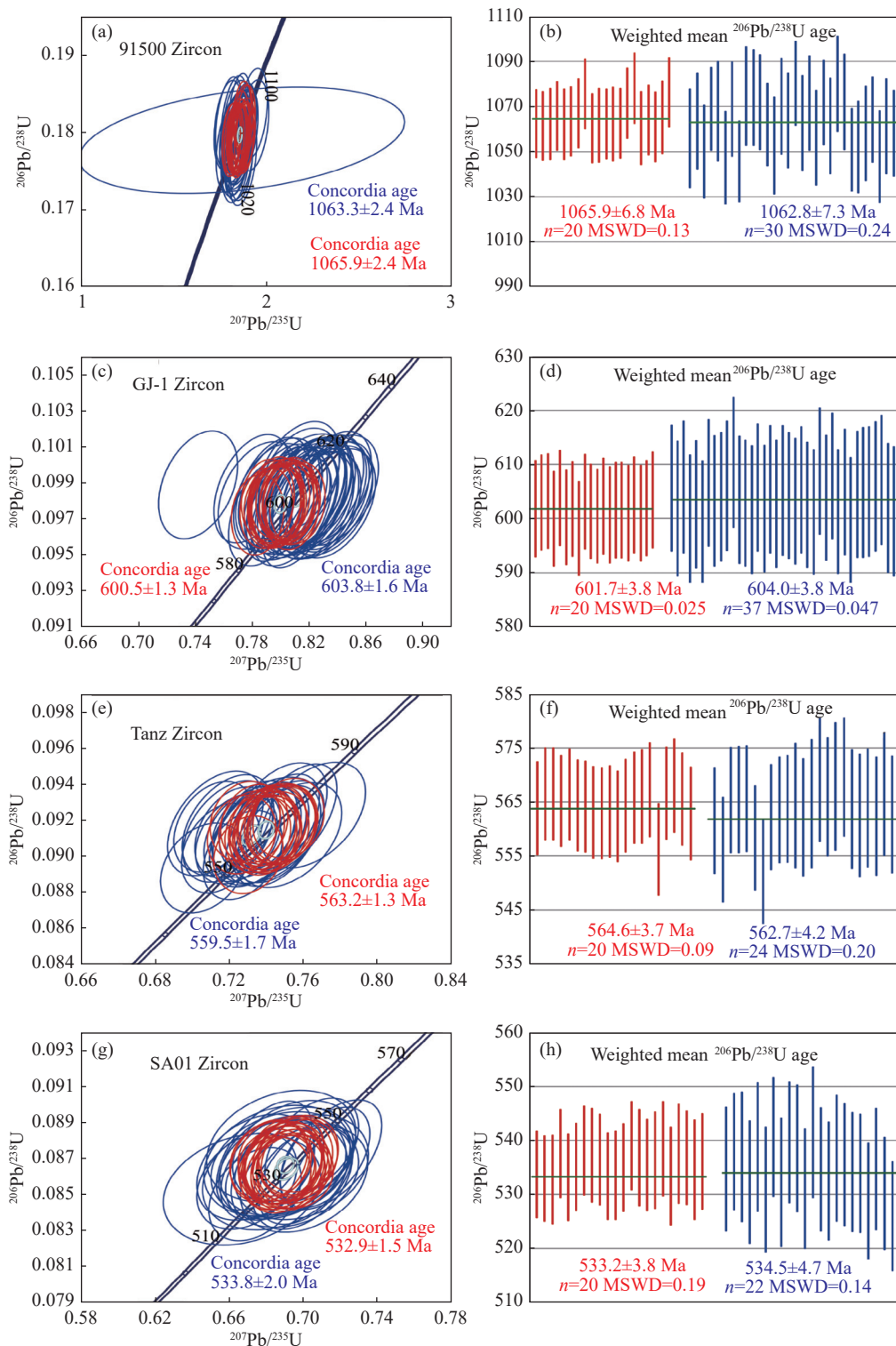
Tanz 镐石: 测试样品 24 点, 获得单点²⁰⁶Pb/²³⁸U 和²⁰⁷Pb/²³⁵U 年龄分别为 550.3~569.7Ma 和 542.5~577.1Ma, 单点误差分别为 9.7~11.9Ma(1.7%~2.1%) 和 8.1~11.5Ma(1.5%~2.0%)。该样品整体谐和年龄为 559.5 ± 1.7 Ma(图 1e), ²⁰⁶Pb/²³⁸U 加权平均年龄为 562.7 ± 4.2 Ma(图 1f), 与推荐年龄在误差范围内一致。

SA01 镐石: 测试样品 22 点, 获得单点²⁰⁶Pb/²³⁸U 和²⁰⁷Pb/²³⁵U 年龄分别为 526.0~541.6Ma 和 518.8~547.8Ma, 单点误差分别为 10.4~12.1Ma (1.9%~2.3%) 和 9.5~17.2Ma(1.7%~3.3%)。该样品整体谐和年龄为 533.8 ± 2.0 Ma(图 1g), ²⁰⁶Pb/²³⁸U 加权平均年龄为 534.5 ± 4.7 Ma(图 1h), 与推荐年龄在误差范围内一致。

Temora1 镐石: 测试样品 26 点, 获得单点²⁰⁶Pb/²³⁸U 和²⁰⁷Pb/²³⁵U 年龄分别为 405.8~426.6Ma 和 404.2~456.4Ma, 单点误差分别为 8.1~10.0Ma (1.9%~2.3%) 和 7.0~16.5Ma(1.6%~3.8%)。该样品整体谐和年龄为 417.5 ± 1.5 Ma(图 2a), ²⁰⁶Pb/²³⁸U 加权平均年龄为 416.7 ± 3.4 Ma(图 2b), 与推荐年龄在误差范围内一致。

Plešovice 镐石: 测试样品 30 点, 其中 2 个点分析结果可能受到蛻晶作用或包裹体影响, ²⁰⁷Pb/²³⁵U 明显偏高外, 其余 28 点单点²⁰⁶Pb/²³⁸U 和²⁰⁷Pb/²³⁵U 年龄分别为 326.4~339.6Ma 和 321.0~342.4Ma, 单点误差分别为 5.2~7.3Ma(1.5%~2.1%) 和 5.1~6.8Ma(1.4%~2.1%)。谐和图上除了受影响的 2 个点偏离谐和线, 其余各点的谐和年龄为 334.6 ± 1.0 Ma(图 2c), ²⁰⁶Pb/²³⁸U 加权平均年龄为 335.8 ± 2.5 Ma(图 2d), MSWD=0.29, 与推荐值在误差范围内一致。

Qinghu 镐石: 测试样品 20 点, 获得单点²⁰⁶Pb/²³⁸U 和²⁰⁷Pb/²³⁵U 年龄分别为 156.3~164.9Ma 和 154.3~176.4Ma, 单点误差分别为 2.9~3.2Ma (1.8%~1.9%) 和 3.1~4.1Ma(2.0%~2.5%)。该样品整体谐和年龄为 160.1 ± 0.6 Ma(图 2e), ²⁰⁶Pb/²³⁸U 加权平均年龄为 160.5 ± 1.3 Ma(图 2f), 与推荐年龄在误差范围内一致。



图中红色数据点为仅测定锆石 U-Pb 同位素方法定年结果; 蓝色数据点为年龄和微量元素含量同时检测方法定年结果。

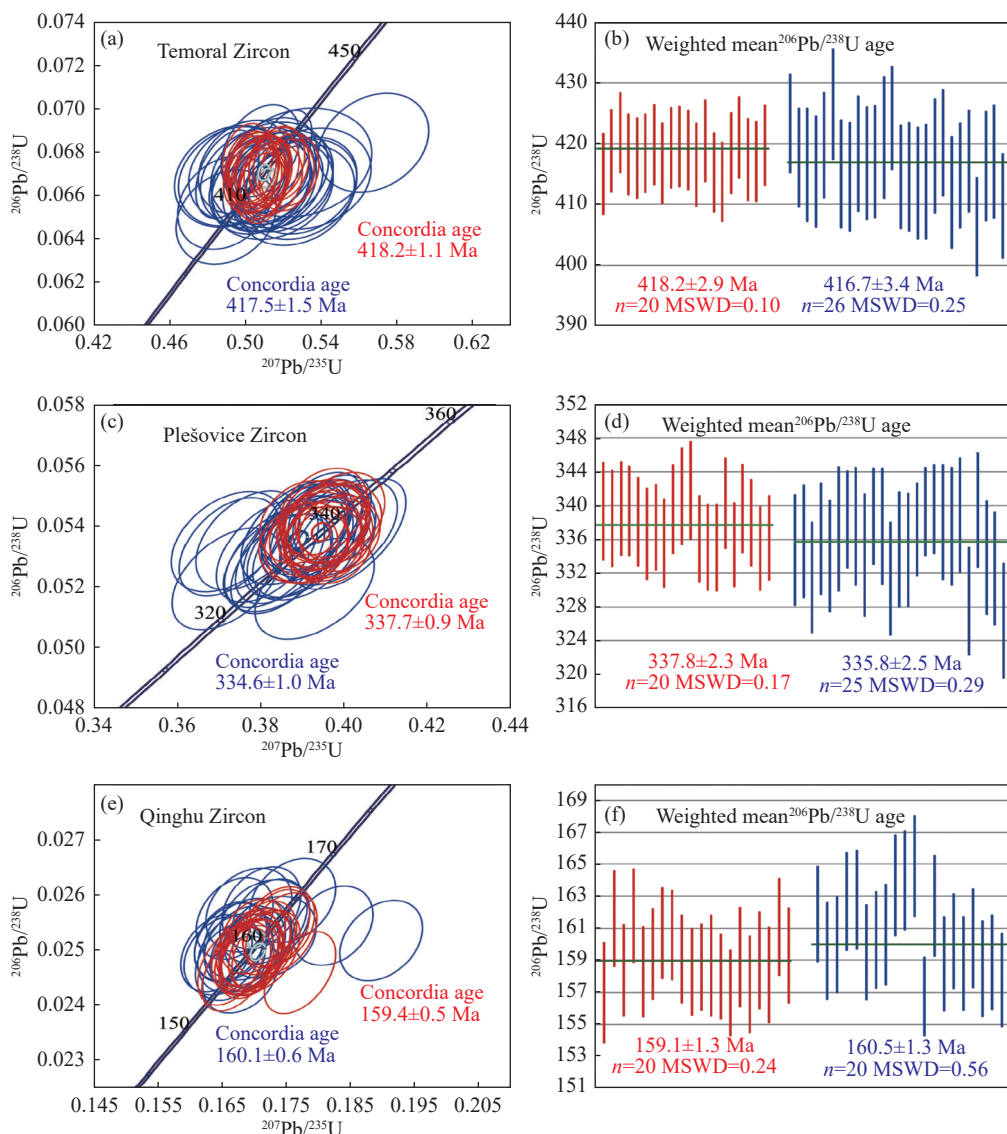
图1 LA-SF-ICP-MS 锆石 U-Pb 定年结果 (激光斑束 $25\mu\text{m}$)

Fig. 1 Zircon U-Pb dating results by LA-SF-ICP-MS; Red data measured only U-Pb isotopes, while blue data determined U-Pb and key trace elements simultaneously (laser spot size $25\mu\text{m}$).

2.2 LA-SF-ICP-MS 仅测定锆石 U-Pb 年龄结果

为探讨 LA-SF-ICP-MS 锆石 U-Pb 年龄和微量

元素含量同时检测对于年龄结果的影响, 本文在相同实验条件下, 仅检测 U-Pb 定年相关同位素, 每个



图中红色数据点为仅测定锆石 U-Pb 同位素方法定年结果；蓝色数据点为年龄和微量元素含量同时检测方法定年结果。

图2 LA-SF-ICP-MS 锆石 U-Pb 定年结果 (激光斑束 $25\mu\text{m}$)

Fig. 2 Zircon U-Pb dating results by LA-SF-ICP-MS; Red data measured only U-Pb isotopes, while blue data determined U-Pb and key trace elements simultaneously (laser spot size $25\mu\text{m}$).

表2 两种不同方法锆石 U-Pb 定年结果对比

Table 2 Zircon U-Pb dating results by LA-(SF)ICP-MS with two methods.

标准样品	仅 U-Pb 定年方法							U-Pb 定年+测定微量元素含量方法								
	$^{206}\text{Pb}/^{238}\text{U}$		$^{207}\text{Pb}/^{235}\text{U}$		谐和年龄 (Ma)	加权平均年龄 (Ma)	$^{206}\text{Pb}/^{238}\text{U}$		$^{207}\text{Pb}/^{235}\text{U}$		谐和年龄 (Ma)	加权平均年龄 (Ma)				
	年龄 (Ma)	2σ (%)	年龄 (Ma)	2σ (%)			年龄 (Ma)	2σ (%)	年龄 (Ma)	2σ (%)						
91500	1045.3 ~ 1076.8	15.0 ~ 16.2	0.8	1047.7 ~ 1106.4	0.8 ~ 11.7	1.3	1065.9 ± 2.4	1065.4 ± 6.8	1045.7 ~ 1080.5	20.3 ~ 22.7	1.0	1044 ~ 1093	14.7 ~ 21.7	1.2	1063.3 ± 2.4	1062.5 ± 7.3
GJ-1	598.2 ~ 603.9	8.6 ~ 8.9	0.2	587.6 ~ 603.5	6.9 ~ 7.7	0.6	600.5 ± 1.3	601.7 ± 3.8	599 ~ 610	11.4 ~ 12.4	0.4	563 ~ 618	9.8 ~ 12.7	1.8	603.8 ± 1.6	604.0 ± 3.8
Tanz	556.3 ~ 568.1	8.3 ~ 8.6	0.5	554.6 ~ 569.4	6.9 ~ 7.3	0.8	563.2 ± 1.3	564.6 ± 3.7	550 ~ 570	10.9 ~ 11.9	0.8	546 ~ 577	9.1 ~ 11.5	1.6	559.5 ± 1.7	562.7 ± 4.2
SA01	525.0 ~ 539.6	7.9 ~ 9.6	0.6	527.8 ~ 537.5	7.8 ~ 9.3	0.5	532.9 ± 1.5	533.2 ± 3.8	526 ~ 542	10.1 ~ 12.1	0.8	519 ~ 548	10 ~ 17.2	1.4	533.8 ± 2.0	534.5 ± 4.7
Temoral	413.8 ~ 421.9	6.5 ~ 6.8	0.5	412.6 ~ 427.2	5.6 ~ 7.3	1.0	418.2 ± 1.1	418.2 ± 2.9	401 ~ 427	8.1 ~ 11.3	1.0	404 ~ 456	7 ~ 19.7	2.7	417.5 ± 1.5	416.7 ± 3.4
Plešovice	333.9 ~ 341.8	4.8 ~ 6.4	0.6	330.1 ~ 340.9	4.4 ~ 5.8	0.6	337.7 ± 0.9	337.8 ± 2.3	326 ~ 340	4.8 ~ 6.9	1.0	321 ~ 342	4.8 ~ 6.9	1.8	334.6 ± 1.0	335.8 ± 2.5
Qinghu	161.8 ~ 156.6	2.6 ~ 3.1	0.9	165.5 ~ 156.2	2.7 ~ 3.2	1.3	159.4 ± 0.5	159.1 ± 1.3	156.3 ~ 164.9	2.9 ~ 3.2	1.4	154.3 ~ 176.4	3.1 ~ 4.1	3.3	160.1 ± 0.6	160.5 ± 1.3

表3 LA-SF-ICP-MS锆石多元素同时分析微量元素定量结果

Table 3 Trace element results measured by LA-SF-ICP-MS, determining U-Pb and key trace elements simultaneously.

元素	检出限 ($\mu\text{g/g}$)	NIST612		KL2-G		91500		SA01		GJ-1	Plešovice	Qinghu	Tanz	Temoral				
		平均值 ($\mu\text{g/g}$)	RSD (%)	平均值 ($\mu\text{g/g}$)	RSD (%)	Si 内标 ($\mu\text{g/g}$)	Zr 内标 ($\mu\text{g/g}$)	文献值 [⁴⁸] ($\mu\text{g/g}$)	Si 内标 ($\mu\text{g/g}$)	Zr 内标 ($\mu\text{g/g}$)	文献值 [³⁵] ($\mu\text{g/g}$)							
Ti	0.302	40.3	4.8	8.5	14053	1.0	8.4	5.9±2.5	5.1±2.8	6±1	12.1±3.49	11.2±1.08	12.1±0.3	3.6±1.57	87.8±21.4	17.2±3.78	15.1±2.68	12.4±1.97
Y	0.025	40.1	1.1	4.8	23.8	1.5	6.5	124±5.2	117±3	140±1.4	402±14.9	382±6.67	—	284±10.3	501±121	700±153	183±10.8	1063±307
La	0.020	36.8	1.4	2.2	12.1	1.2	8.0	0.03±0.03	0.03±0.04	0.006±0.003	0.104±0.02	0.096±0.03	0.108±0.02	<	0.162±0.173	10.3±1.77	0.02±0.006	0.072±0.027
Ce	0.017	38.3	1.1	0.3	30.0	1.4	7.3	2.3±0.08	2.1±0.14	2.6±0.3	16.8±0.566	15.4±0.464	17.8±1.1	14±0.6	2.99±1.35	0.245±0.203	0.245±0.112	3.67±0.687
Pr	0.013	38.1	1.1	0.7	4.3	1.6	6.9	0.03±0.02	0.02±0.01	0.024±0.015	0.615±0.043	0.586±0.037	0.67±0.04	0.034±0.008	2.5±1.21	1.59±0.691	0.963±0.118	0.184±0.076
Nd	0.056	36.8	1.7	3.6	19.7	1.9	8.9	0.23±0.05	0.2±0.09	0.24±0.04	7.89±0.482	7.94±0.328	8.94±0.51	0.655±0.19	2.5±1.32	3.73±1.4	0.05±0.01	2.64±1.04
Sm	0.045	38.9	1.6	3.2	5.4	2.6	2.6	0.44±0.06	0.41±0.1	0.5±0.08	8.39±0.307	9.31±0.436	10.1±0.47	1.61±0.29	4.05±1.32	0.389±0.177	1.52±0.197	4.38±1.71
Eu	0.024	36.4	0.8	2.4	1.8	2.7	7.2	0.25±0.02	0.23±0.04	0.24±0.03	5.04±0.171	5.34±0.136	6.04±0.36	1.16±0.129	1.08±0.418	0.389±0.177	0.951±0.315	
Gd	0.073	38.6	2.6	3.4	5.6	4.8	5.9	2.2±0.08	2.1±0.19	2.2±0.3	23±1.06	23.7±0.777	25.1±1.5	7.48±0.53	14.4±4.42	14.8±4.66	11.6±1.33	20.8±7.31
Tb	0.017	38.1	1.0	1.4	0.8	4.1	9.0	0.74±0.04	0.74±0.05	0.86±0.07	5.34±0.271	5.4±0.15	5.94±0.36	2.15±0.153	5.24±1.46	5.5±1.51	2.9±0.333	7.32±2.56
Dy	0.062	37.3	1.7	5.0	4.7	3.4	9.6	10±0.42	10±0.48	12±1	49.4±0.869	50.4±1.5	53.3±3	22.2±0.936	58.3±15.6	65.8±16.7	25.2±2.23	89.1±30.5
Ho	0.011	39.5	1.3	3.1	0.9	3.2	4.2	4.1±0.14	4.1±0.14	4.8±0.4	14±0.421	13.7±0.244	14.9±0.9	7.55±0.245	15.6±3.87	23.1±5.42	6.17±0.382	34.4±10.7
Er	0.041	39.6	2.1	4.2	2.5	4.6	3.3	23±0.86	22±0.76	25±3	55.7±2.37	52.2±1.32	56.2±2.1	32.9±1.4	56.1±13.2	104±21.6	21.2±1.25	16.2±4.5
Tm	0.009	38.7	1.0	5.1	0.4	5.6	7.0	6.7±0.21	6±0.17	6.9±0.4	10.1±0.478	11±0.236	11.3±0.7	7.1±0.359	10.2±2.45	25±5.18	3.79±0.254	34.4±8.54
Yb	0.071	40.1	2.5	2.2	2.0	4.1	3.2	78±1.9	71±2.2	74±4	87.7±3.24	105±2.71	107±4.6	72.2±4.3	78.9±21.2	245±46.6	31.3±3.03	33.4±76.3
Lu	0.011	38.0	1.3	2.7	0.3	5.5	5.4	12±0.5	9.6±0.26	13±1	16.5±0.588	13.1±0.297	15.4±0.7	14.5±1.15	8.27±2.14	40.5±6.4	4.02±0.399	66.4±14
Hf	0.043	37.9	1.3	3.2	3.8	4.2	4.2	6027±325	5424±85	5900±300	9650±610	8647±151	10019±579	7220±297	10420±546	10027±359	10925±617	8252±538
Pb	0.015	38.9	1.2	0.8	1.9	3.0	6.5	15±0.41	13±0.36	15±2	13±0.4	11.2±0.591	22.5±9.7	43.7±2.28	53±18.2	20.7±5.23	35.2±2.18	13.2±6.16
Th	0.004	39.1	1.1	3.6	1.0	3.3	4.1	25±0.8	24±0.55	30±3	139±4.44	128±2.18	140±11	7.59±0.366	97.8±42.8	357±93	71.2±7.87	72.6±33.8
U	0.002	37.8	1.2	1.1	0.6	1.5	17.5	71±2.4	67±2.2	80±8	105±3.63	94.4±4.86	114±13	430±18	972±345	657±159	366±15.9	169±78.6

注:“—”表示文献未报道;“<”表示测试数据低于方法检出限。

样品测试 20 点, U-Pb 年龄结果见图 1、图 2 和表 2。

91500 锆石: 单点 $^{206}\text{Pb}/^{238}\text{U}$ 和 $^{207}\text{Pb}/^{235}\text{U}$ 年龄分别为 1045.3 ~ 1076.8 Ma 和 1047.7 ~ 1106.4 Ma, 单点误差分别为 15.0 ~ 16.2 Ma (~ 1.4%) 和 10.8 ~ 11.7 Ma (~ 1.1%)。该样品整体谐和年龄为 1065.9 ± 2.4 Ma (图 1a), $^{206}\text{Pb}/^{238}\text{U}$ 加权平均年龄为 1065.4 ± 6.8 Ma (图 1b)。

GJ-1 锆石: 单点 $^{206}\text{Pb}/^{238}\text{U}$ 和 $^{207}\text{Pb}/^{235}\text{U}$ 年龄分别为 598.2 ~ 603.9 Ma 和 587.6 ~ 603.5 Ma, 单点误差分别为 8.6 ~ 8.9 Ma (~ 1.4%) 和 6.9 ~ 7.7 Ma (1.2% ~ 1.3%)。该样品整体谐和年龄为 600.5 ± 1.3 Ma (图 1c), $^{206}\text{Pb}/^{238}\text{U}$ 加权平均年龄为 601.7 ± 3.8 Ma (图 1d)。

Tanz 锆石: 单点 $^{206}\text{Pb}/^{238}\text{U}$ 和 $^{207}\text{Pb}/^{235}\text{U}$ 年龄分别为 556.3 ~ 568.1 Ma 和 554.6 ~ 569.4 Ma, 单点误差分别为 8.3 ~ 8.6 Ma (~ 1.5%) 和 6.9 ~ 7.3 Ma (1.2% ~ 1.3%)。该样品整体谐和年龄为 563.2 ± 1.3 Ma (图 1e), $^{206}\text{Pb}/^{238}\text{U}$ 加权平均年龄为 564.6 ± 3.7 Ma (图 1f)。

SA01 锆石: 单点 $^{206}\text{Pb}/^{238}\text{U}$ 和 $^{207}\text{Pb}/^{235}\text{U}$ 年龄分别为 525.4 ~ 539.6 Ma 和 527.8 ~ 537.1 Ma, 单点误差分别为 8.2 ~ 9.2 Ma (~ 1.5%) 和 8.3 ~ 8.8 Ma (1.5% ~ 1.7%)。该样品整体谐和年龄为 532.9 ± 1.5 Ma (图 1g), $^{206}\text{Pb}/^{238}\text{U}$ 加权平均年龄为 533.2 ± 3.8 Ma (图 1h)。

Temoral1 锆石: 单点 $^{206}\text{Pb}/^{238}\text{U}$ 和 $^{207}\text{Pb}/^{235}\text{U}$ 年龄分别为 413.8 ~ 421.9 Ma 和 412.6 ~ 427.2 Ma, 单点误差分别为 6.5 ~ 6.8 Ma (~ 1.5%) 和 5.6 ~ 7.3 Ma (1.3% ~ 1.7%)。该样品整体谐和年龄为 418.2 ± 1.1 Ma (图 2a), $^{206}\text{Pb}/^{238}\text{U}$ 加权平均年龄为 418.2 ± 2.9 Ma (图 2b)。

Plešovice 锆石: 单点 $^{206}\text{Pb}/^{238}\text{U}$ 和 $^{207}\text{Pb}/^{235}\text{U}$ 年龄分别为 335.0 ~ 341.8 Ma 和 333.7 ~ 340.9 Ma, 单点误差分别为 4.9 ~ 5.8 Ma (1.3% ~ 1.5%) 和 4.6 ~ 5.2 Ma (1.5% ~ 1.7%)。该样品整体谐和年龄为 337.7 ± 0.9 Ma (图 2c), $^{206}\text{Pb}/^{238}\text{U}$ 加权平均年龄为 337.8 ± 2.3 Ma (图 2d)。

Qinghu 锆石: 单点 $^{206}\text{Pb}/^{238}\text{U}$ 和 $^{207}\text{Pb}/^{235}\text{U}$ 年龄分别为 161.8 ~ 156.6 Ma 和 165.5 ~ 156.2 Ma, 单点误差分别为 2.6 ~ 3.1 Ma (1.6% ~ 2.0%) 和 2.7 ~ 3.2 Ma (1.7% ~ 2.0%)。该样品整体谐和年龄为 159.4 ± 0.5 Ma (图 2e), $^{206}\text{Pb}/^{238}\text{U}$ 加权平均年龄为 159.1 ± 1.3 Ma (图 2f)。

2.3 LA-SF-ICP-MS 定年与多元素含量同时测试方法和仅 U-Pb 定年方法对比

受 SF-ICP-MS 磁场定位时间的影响, 本文中仅测 U-Pb 相关同位素方法质谱单次扫描时间 0.306 s,

在 40 s 的激光剥蚀样品时间内, 采集元素信号强度数据 134 组; 而 U-Pb 年龄与微量元素含量同时分析方法中质谱单次扫描时间 0.857 s, 在 40 s 激光采样时间内获得有效信号强度数据 47 组。

图 1 和图 2 对两种方法定年结果的精密度和准确度进行了直观地比较, 相较之下, 仅检测 U-Pb 同位素方法定年结果数据点误差更小, 且数据点更为集中。

LA-SF-ICP-MS 仅检测 U-Pb 同位素方法定年结果 $^{206}\text{Pb}/^{238}\text{U}$ 和 $^{207}\text{Pb}/^{235}\text{U}$ 年龄误差分别为 1.5% 和 1.3%, 单点 $^{206}\text{Pb}/^{238}\text{U}$ 和 $^{207}\text{Pb}/^{235}\text{U}$ 年龄一致性较好, RSD 值分别为 0.2% ~ 0.9% 和 0.5% ~ 1.3%; 相比之下, U-Pb 定年和多元素含量同时检测方法获得 $^{206}\text{Pb}/^{238}\text{U}$ 和 $^{207}\text{Pb}/^{235}\text{U}$ 年龄误差略有增大, 分别为 1.9% 和 1.7%, 单点年龄离散度增大, $^{206}\text{Pb}/^{238}\text{U}$ 和 $^{207}\text{Pb}/^{235}\text{U}$ 年龄 RSD 值分别为 0.4% ~ 1.4% 和 1.2% ~ 3.3%, 其中 $^{207}\text{Pb}/^{235}\text{U}$ 年龄 RSD 值增大明显。

为探讨两种方法测定年龄结果精密度变化可能原因, 本文以 91500 锆石为例, 统计了相同实验条件下, 两种方法测定 ^{206}Pb 、 ^{207}Pb 信号强度及 $^{238}\text{U}/^{206}\text{Pb}$ 信号比值的相对标准偏差 (RSD)。其中, 仅检测 U-Pb 同位素方法采集 ^{206}Pb 、 ^{207}Pb 信号和 $^{238}\text{U}/^{206}\text{Pb}$ 信号比值的 RSD 分别为 13%、13% 和 5.2%, 而多元素含量同时检测方法获得 ^{206}Pb 、 ^{207}Pb 信号和 $^{238}\text{U}/^{206}\text{Pb}$ 同位素信号比值的 RSD 分别为 14%、19% 和 9.3%。多元素同时采集延长了质谱单次扫描时间, 在一定程度上对于检测同位素的信号强度及比值稳定性造成影响, 尤其是对于低含量同位素如 ^{207}Pb 的影响更为明显。两种测试方法同位素信号及比值变化特征与 U-Pb 定年结果变化特征相一致。综合考虑数据处理过程中年龄不确定度计算方法和影响因素^[43-46], 因此, 多元素同时检测对于同位素信号强度稳定性的影响可能是造成最终定年结果误差变大的主要原因。

锆石 LA-ICP-MS 定年过程中, 多种因素都会对测试结果的精密度和准确度造成影响, 例如测试仪器状态、标准样品推荐值、数据处理方法及软件应用等。目前一般认为 LA-ICP-MS 锆石 U-Pb 定年结果精密度为 1% ~ 2%, 相对于推荐年龄 LA-ICP-MS 测试年龄结果偏差 (准确度) 可达到 1%^[43-46]。本文实验结果表明, 尽管多元素同时检测可造成单点锆石 U-Pb 年龄结果的变化范围增大, 但数据结果精密度仍优于 2%, 并且多元素同时检测对于样品的谐和年龄和 $^{206}\text{Pb}/^{238}\text{U}$ 加权平均年龄的准确性没有影

响——仅检测 U-Pb 同位素方法获得各样品谐和年龄和 $^{206}\text{Pb}/^{238}\text{U}$ 加权平均年龄相对 TIMS 年龄偏差均小于 0.5%, 多元素同时检测分析方法获得各样品谐和年龄和 $^{206}\text{Pb}/^{238}\text{U}$ 加权平均年龄相对 TIMS 年龄偏差分别小于 1.0% 和 0.7%, 完全满足 U-Pb 同位素地质年代学测试要求, 同时, 高精度和高空间分辨率的定年方法为精细刻画复杂地质过程提供技术支持^[46]。

2.4 LA-SF-ICP-MS 锆石定年同时分析微量元素定量结果准确性分析

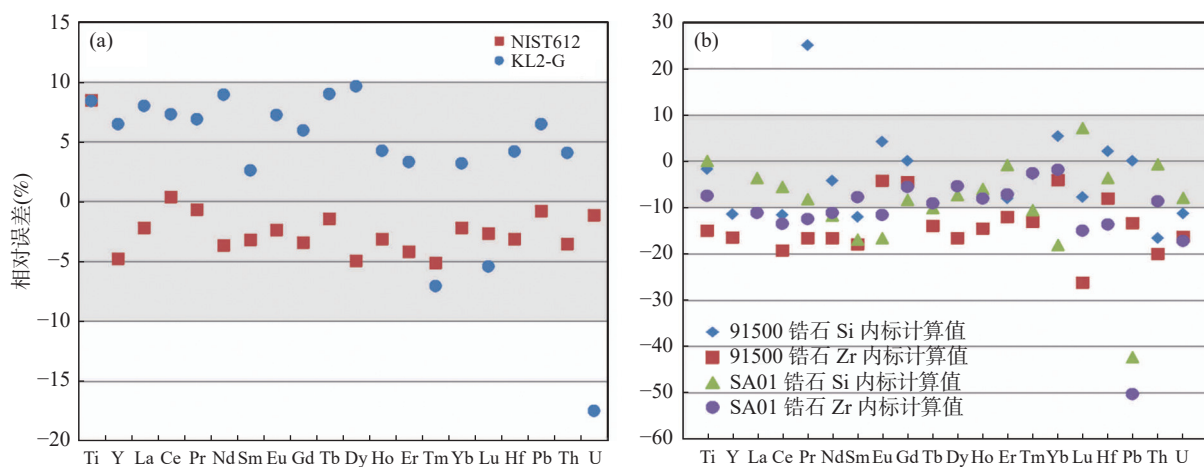
采用 LA-SF-ICP-MS 测定锆石 U-Pb 年龄的同时, 对锆石中 Si、Ti、Y、Zr、Hf、REEs、Pb、Th 和 U 等关键主、微量元素进行定量分析。实验采用 NIST610 作为微量元素含量分析外标物质, 数据处理选择 Si(SiO₂ 含量 32.8%) 或者 Zr(ZrO₂ 含量 67.2%) 作为内标元素, 分析结果列于表 3。

稀土元素检出限在 11~73ng/g 之间, 大部分小于 20ng/g, 其中 La 和 Pr 检出限分别为 20ng/g 和 13ng/g, 这两个元素在多数锆石中极度亏损, 较低的检出限有利于这两个元素的检测准确。Ti 检出限最高达 302ng/g, Pb、Th、U 检出限最低, 分别为 15ng/g、4ng/g 和 2ng/g。本方法的检出限能够满足锆石中关键微量元素准确定量需求。

由于天然锆石中微量元素分布的不均匀性, 因此, 对锆石微量元素含量的测定结果难以反映分析方法的精确度和准确度。本实验中随测 NIST612 和 KL2-G 作为质量监控样品。10 组监控样品结果

表现良好的精密度(图 3a), NIST612 中除 Ti 元素 RSD 略高外(4.8%), 其余元素 RSD 值小于 3%; KL2-G 中含量较低的 Tm 和 Lu 的 RSD 值 ~ 5%, 其余元素 RSD 值均小于 5%。检测结果平均值与标准样品推荐值相比较, NIST612 中 Ti 的相对误差(8.5%)较高, 其余元素的相对误差均小于 5%, 准确度较高; 而 KL2-G 中各元素的相对误差多在 5%~10% 之间, U 的相对误差最大达 ~ 17%。虽然 KL2-G 中各元素含量相对较低, 但良好的测试精密度表明较高的相对误差更可能是由于 NIST610 与 KL2-G 之间的基体差异的影响。尽管目前锆石微量元素分析中常采用 NIST610 作为标准样品, 但研究表明 NIST 系列标准样品与天然矿物基体差异明显^[47], 其微量元素含量明显高于锆石, 尤其是 LREEs 含量, 因此对于锆石微量元素含量准确定量有待于进一步研究。总体上, 本文建立的方法对于 NIST612 和 KL2-G 可获得稳定、准确的分析结果。

内标元素的选择是影响 LA-ICP-MS 分析结果准确性的主要因素。尽管研究表明 LA-ICP-MS 测定锆石微量元素含量过程中, 在 NIST610 为外标条件下, Zr 相对于 Si 更适合作为内标元素^[47]。本实验中分别采用 Si 和 Zr 作为内标元素进行定量分析, 所有锆石样品定量结果显示采用 Si 作为内标元素计算结果总体上略高于 Zr 作为内标计算结果(图 3b)。对于 91500 和 SA01 样品, 采用 Si 内标各元素分析结果与文献^[35]和^[48]推荐值相对误差多小于 10%, 而采用 Zr 内标结果相对误差在 10%~20% 之间。



相对误差=(测定值-推荐值)/推荐值; 灰色区域为±10%。

图3 (a)NIST612 和 KL2-G 测定值与文献推荐值相对误差; (b)91500 和 SA01 锆石微量元素含量测定值与文献推荐值相对误差
Fig. 3 (a) Relative errors of NIST612 and KL2-G between measured value and reference value; (b) Relative errors of 91500 and SA01 zircon between measured value and reference value.

另外,由于锆石与采用的标准样品中 Zr 含量差异悬殊,在使用高扩散空间匀化装置条件下,锆石分析后需要长时间吹扫以降低仪器中 Zr 背景值,且可能影响标准样品中 Zr 检测准确性。尽管检测 Si 会增大 SF-ICP-MS 磁场变化范围,在有效时间内减少扫描次数(约减少 5 组数据),但综合实验结果,对于 U-Pb 定年结果及误差没有明显影响,因此本实验方法中检测 Si 作为内标元素。

91500、SA01、GJ-1 和 Tanz 颗粒内部微量元素均一性较好,检测结果除 Ti、La 误差略高外,其余元素误差均小于 10%; Plešovice 颗粒内部元素均一性较差,所有检测元素的相对误差均大于 10%; Qinghu 和 Temora1 锆石由于检测点位于不同颗粒,因此微量元素含量结果相差较大。总体上,按照锆石中的 U 平均含量,91500<SA01<Temora1<Tanz<GJ-1 <Qinghu<Plešovice, 其中 Qinghu、Temora1、91500 和 SA01 放射性 Pb 总量相当(大约 10~13 $\mu\text{g/g}$), Tanz 锆石放射性 Pb 总量 ~ 34 $\mu\text{g/g}$, 略低于 GJ-1 (~ 42 $\mu\text{g/g}$); Plešovice 锆石中放射性 Pb 总量较高且变化较大,平均 ~ 52 $\mu\text{g/g}$ 。实验中可综合质谱仪灵敏度、检测器模式转换和样品中 U-Pb 含量,选择合适的标准样品。

在球粒陨石标准化图解上,所有锆石样品具有一致的亏损 LREEs 富集 HREEs 的特征,明显的 Ce 正异常,Eu 异常差别明显, Temora1 和 Plešovice 具有明显的负 Eu 异常(图 4 中 a, c), Tanz 锆石呈现弱负 Eu 异常(图 4b), GJ-1 和 SA01 中 Eu 呈现弱负异常或无异常(图 4 中 a, b)。

微量元素替代进入锆石中可能对锆石结构特征造成影响, LA-ICP-MS 分析过程中影响激光剥蚀效率,从而影响 U-Pb 年龄结果^[49-50],因此,在锆石 U-Pb 定年过程中可以根据以上各个锆石标准样品的

微量元素特征,结合仪器工作条件选择与待测锆石样品基体更为匹配的标准,以降低由此可能带来的误差。

3 结论

采用激光剥蚀-扇形磁场高分辨等离子体质谱(LA-SF-ICP-MS)建立了锆石 U-Pb 年龄与微量元素含量同时检测分析方法,并对常用的锆石 U-Pb 定年标准样品进行分析。分析结果表明:相对于仅检测 U-Pb 相关同位素方法, U-Pb 定年及微量元素同时检测方法在一定程度上影响了 U-Pb 同位素信号稳定性,尤其是对低含量元素/同位素信号稳定性的影响更为明显,进而对 U-Pb 定年结果精密度产生影响。相对仅检测 U-Pb 同位素分析方法结果,多元素同时分析 $^{206}\text{Pb}/^{238}\text{U}$ 年龄和 $^{207}\text{Pb}/^{235}\text{U}$ 年龄变化范围变大,其中 $^{206}\text{Pb}/^{238}\text{U}$ 年龄 RSD 值从 0.2%~0.9% 增大至 0.4%~1.4%; $^{207}\text{Pb}/^{235}\text{U}$ 年龄 RSD 值从 0.5%~1.3% 增大至 1.2%~3.3%,单点年龄误差从 ~1.5% 增大至 ~2.0%。尽管如此,多元素同时检测方法不会对样品最终年龄结果产生明显影响,该方法测定各样品谐和年龄和 $^{206}\text{Pb}/^{238}\text{U}$ 加权平均年龄与仅检测 U-Pb 同位素方法测定年龄结果在误差范围内一致,与 TIMS 年龄结果偏差均小于 1%,完全满足地质年代学分析需求。同时,测定各锆石样品中微量元素含量值与文献报道范围吻合,其中 91500 和 SA01 样品中各元素测定值与文献报道值相对误差小于 10%。综合以上分析结果,采用 LA-SF-ICP-MS 建立的分析方法克服了高分辨质谱仪扫描速度慢的缺点,可以同时准确测定锆石的 U-Pb 年龄和关键微量元素含量。

尽管 LA-ICP-MS 锆石 U-Pb 定年方法已十分成熟,但提高其空间分辨率,并且在有限的分析空间获

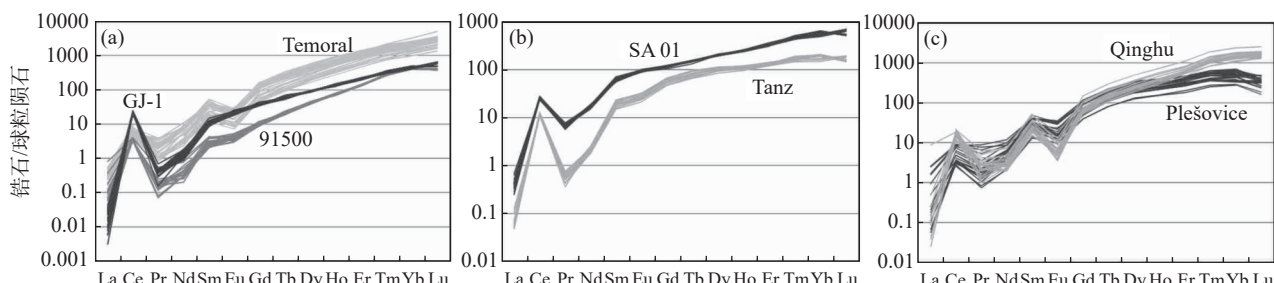


图4 锆石样品稀土元素配分模式图

Fig. 4 Rare earth element distribution patterns for zircon samples. Chondrite normalization values are after Sun and McDonough (1989).

得更多的原位元素/同位素信息是研究者不变的追求。LA-SF-ICP-MS 同时进行 U-Pb 定年和微量元素含量分析,一方面可以充分利用高分辨质谱高灵敏度特征实现高空间分辨率分析,另一方面原位微量元素含量的准确测定可以获得更多的地质信息,为精细

刻画地质演化环境和过程提供丰富地球化学数据。

致谢: 中国科学院地质与地球物理研究所王浩副研究员提供 SA01 锆石样品; 中国地质大学(武汉)罗涛副研究员提供 Tanz 锆石样品,在此表示感谢!

Simultaneous Determination of U-Pb Age and Trace Elements of Zircon by Laser Ablation Sector Field Inductively Coupled Plasma-Mass Spectrometry

ZHAO Linghao, SUN Dongyang, HU Mingyue, YUAN Jihai, FAN Chenzi, ZHAN Xiuchun

(Key Laboratory of *in situ* Elemental Micro-probe and Speciation Analysis, China Geological Survey;

National Research Center for Geoanalysis, Beijing 100037, China)

HIGHLIGHTS

- (1) Simultaneous determination of zircon U-Pb age and multiple trace element contents by LA-SF-ICP-MS can affect the stability of U-Pb isotope signals and ratios, leading to an increased uncertainty in single-analysis U-Pb dating results. However, it has no effect on the accuracy of the concordant ages due to multi-point analysis, and the precision is slightly reduced.
- (2) Simultaneous measurement of zircon U-Pb ages and trace element contents using LA-SF-ICP-MS, yields zircon U-Pb age deviations of less than 1% and deviations in key trace elements such as REE, Ti, Hf, Pb, Th, and U of less than 10%.
- (3) Solely determining zircon U-Pb ages by LA-SF-ICP-MS effectively reduces uncertainty introduced by single-analyses isotope ratio measurement, improving dating precision ($2\sigma < 2\%$) and accuracy (RSE $< 0.5\%$).

ABSTRACT: Laser ablation sector field inductively coupled plasma-mass spectrometry (LA-SF-ICP-MS) is widely applied in U-Pb dating of zircon due to its remarkable sensitivity. However, the utilization of a magnetic sector mass analyzer imposes constraints on its scanning speeds, potentially affecting the concurrent acquisition of U-Pb isotopes and other trace elements. Here a method for simultaneous zircon U-Pb dating and key trace elements quantifying by LA-SF-ICP-MS were developed. Seven zircon U-Pb standard samples were measured to assess the method's feasibility. Experimental data indicate that simultaneous collection of U-Pb isotopes and other trace elements may decrease signal stability, particularly for low-content isotopes like ^{207}Pb , which in turn leads to an increased age uncertainty and dispersion for single analyses. However, the accuracy of the concordance age and weighted mean $^{206}\text{Pb}/^{238}\text{U}$ age of each sample, and the statistical results of all data points, are not affected significantly. Compared to TIMS ages, the discordance in these ages across all samples remains below 1.0% and 0.7%, respectively, meeting the requirements of U-Pb geological dating. Furthermore, the determination of key trace elements in zircon samples shows relative errors to recommended values of less than 10%. LA-SF-ICP-MS can accurately determine both zircon U-Pb ages and trace element contents simultaneously. The BRIEF REPORT is available for this paper at <http://www.ykcs.ac.cn/en/article/doi/10.15898/j.ykcs.202309110151>.

KEY WORDS: laser ablation sector field inductively coupled plasma-mass spectrometry; zircon; U-Pb dating; trace element

BRIEF REPORT

Significance: Zircon ($ZrSiO_4$) is a common accessory mineral in both terrestrial and extraterrestrial rocks. It serves as the most frequently utilized mineral in determining the age, origin, and thermal history of rocks through U-Pb geochronology, primarily due to its high closure temperature, resistance to alteration, high uranium content, and minimal incorporation of common lead during its crystallization. Apart from age determination, zircon also provides various geochemical information, including trace elements (Ti, REEs), O isotopes, and Zr isotopes. By combining all these data, it assists in constructing metamorphic $P-T-t$ paths, which helps in inferring the mineral growth history, making it an integral component of “Petrochronology” research^[20]. Natural zircon, however, generally exhibits small grains and often possesses intricate internal structural features. Hence, higher analytical spatial resolution and acquiring more in-situ elemental/isotopic information within limited analytical space is crucial.

Laser ablation inductively coupled plasma-mass spectrometry (LA-ICP-MS) is a routine technique for zircon U-Pb dating. The sector field mass spectrometer (SF-ICP-MS) possesses high sensitivity, offering possibilities for high spatial resolution U-Pb dating of zircon^[28-29] and ultra-low uranium mineral content^[21-25, 30]. However, the usage of the magnetic sector mass analyzer results in slower scanning speeds^[27]. Consequently, in the reported zircon U-Pb dating by LA-SF-ICP-MS, typically, only U-Pb-ages-related isotopes are detected, and simultaneous quantitative analysis of key trace elements cannot be conducted.

This study optimized instrument parameters and enhanced signal stability to enable simultaneous determination of U-Pb dating alongside quantification of key elements such as Ti, REEs, and Hf. Seven commonly employed zircon U-Pb standard samples were measured to assess the feasibility of the method and its influence on U-Pb dating results.

Methods: The experiments were carried out at the Key Laboratory of Elemental Microanalysis and Morphology of the China Geological Survey using an ESL NWR 193UC ArF excimer laser and the ELEMENT II sector field inductively coupled plasma-mass spectrometer (SF-ICP-MS, ThermoFisher Scientific, USA).

Helium gas was used as the carrier gas^[39], while 1mL/min of nitrogen was introduced to boost instrument sensitivity^[40]. A signal homogenization device with higher aerosol diffusion space was utilized to improve signal stability. Laser spot size and frequency were 25μm and 8Hz, respectively, with a laser energy density of 3J/cm². SF-ICP-MS was employed in low-resolution mode ($M/\Delta M=300$), with sensitivity of U about 5000cps/(μg·g⁻¹), and signal stability RSD of 1% to 2%, oxide production rates (ThO^+/Th^+) below 0.2%. U-Pb isotopes and key trace elements were measured, including ^{29}Si , ^{49}Ti , ^{89}Y , ^{91}Zr , ^{139}La , ^{140}Ce , ^{141}Pr , ^{146}Nd , ^{147}Sm , ^{151}Eu , ^{157}Gd , ^{159}Tb , ^{163}Dy , ^{165}Ho , ^{166}Er , ^{169}Tm , ^{172}Yb , ^{175}Lu , ^{178}Hf , ^{206}Pb , ^{207}Pb , ^{208}Pb , ^{232}Th , and ^{238}U . The measuring time for ^{206}Pb , ^{208}Pb , ^{232}Th , and ^{238}U was 10ms, ^{207}Pb was 20ms, and the remaining elements were 5ms each, resulting in a total measuring time of 0.87s per reading, with an effective analysis time of 71%. Since most zircons contain no, or extremely low, common lead and single-collector mass spectrometry it makes it challenging to accurately measure ^{204}Pb for common lead correction. ^{202}Hg and ^{204}Pb were not detected to improve the proportion of effective analysis time. Detailed instrument operating condition parameters are provided in Table 1.

The 91500 zircon and NIST610 were used as standard materials for U-Pb isotope ratios and trace element quantitative analysis, respectively. For every 10 unknown sample analyses, a set of standard samples was inserted to correct for fractionation effects. Each spot analysis consisted of a 20s background collection and 40s sample data acquisition and 30s flushing. Raw data were reduced offline using GLITTER 4.0 software package^[41]. All samples shared the same signal interval as the standard zircon 91500 for analysis. Age calculations and Concordia diagram construction were performed by Isoplot/Ex version 2.23^[42]. The uncertainty for all isotope ratios and age values in this study were reported at a 2σ level.

Two methods were used to determine zircon U-Pb ages. Method 1: Only U-Pb-related isotopes were measured, including ^{202}Hg , ^{204}Pb , ^{206}Pb , ^{207}Pb , ^{208}Pb , ^{232}Th , and ^{238}U . Single measuring time was 0.306s per reading, and within the 40s sampling time, data for 134 sets of element signal intensities were collected. Method 2: Simultaneous determination of U-Pb ages and trace elements content, including Ti, REE, Hf, and U-Pb isotopes ^{206}Pb , ^{207}Pb , ^{208}Pb , ^{232}Th , ^{238}U , etc. Single measuring time was 0.857s, and within the 40s sampling time, effective signal intensity data for 47 sets were obtained.

Data and Results: The U-Pb dating results are shown in Fig.1 and Table 2, while the measured trace element contents are presented in Fig.3 and Table 3.

(1) U-Pb dating results comparison

Fig.1 provides a visual comparison of precision and accuracy of the results obtained by these two dating methods. It shows that the dating results from Method 1 exhibit smaller errors, and the data points are more concentrated.

Using LA-SF-ICP-MS with solely U-Pb-related isotope detection, the dating results show an error of 1.5% and 1.3% for $^{206}\text{Pb}/^{238}\text{U}$ and $^{207}\text{Pb}/^{235}\text{U}$, respectively. The consistency of single-point $^{206}\text{Pb}/^{238}\text{U}$ and $^{207}\text{Pb}/^{235}\text{U}$ ages is good, with RSD values ranging from 0.2% to 0.9% and 0.5% to 1.3%, respectively. In contrast, when employing Method 2, the errors for $^{206}\text{Pb}/^{238}\text{U}$ and $^{207}\text{Pb}/^{235}\text{U}$ ages increase slightly to 1.9% and 1.7%, respectively. The dispersion of single-point ages increases as well, with RSD values for $^{206}\text{Pb}/^{238}\text{U}$ and $^{207}\text{Pb}/^{235}\text{U}$ ages ranging from 0.4% to 1.4% and 1.2% to 3.3%, respectively. Particularly, the RSD value for $^{207}\text{Pb}/^{235}\text{U}$ ages notably increases.

To investigate potential causes for the variability in precision between the two methods, the RSD of the signal intensities of ^{206}Pb , ^{207}Pb , and $^{238}\text{U}/^{206}\text{Pb}$ signal ratios of zircon 91500 obtained under the same experimental conditions were statistically analyzed. For Method 1, the RSD values for the collection of ^{206}Pb , ^{207}Pb signals, and $^{238}\text{U}/^{206}\text{Pb}$ signal ratios were 13%, 13%, and 5.2%, respectively. Meanwhile, for method 2, the RSD values for ^{206}Pb , ^{207}Pb signals, and $^{238}\text{U}/^{206}\text{Pb}$ isotope signal ratios were 14%, 19%, and 9.3%, respectively. Simultaneously collecting multiple elements extended the mass spectrometer's single-scan time, which to some extent affected the stability of the detected element/isotope signals and their ratios, especially for low-content isotopes like ^{207}Pb . The fluctuation characteristics of isotopic signals and ratios corresponded to the changes in U-Pb dating results. Considering factors during data processing, age uncertainty calculation methods, and influencing elements^[43-46], it can be inferred that the impact of simultaneous multi-element detection on the stability of isotope signal intensity might be the primary cause for the increased final dating result errors.

Generally, the precision of LA-ICP-MS zircon U-Pb dating results is considered to be within 1% to 2%, while the accuracy of the measured age can reach 1% or better^[43-46]. The experimental results in this study indicate that although simultaneous multi-element detection can increase the range of changes in single-point zircon U-Pb ages, the precision of the data is still better than 2%. Furthermore, simultaneous multi-element detection does not affect the accuracy of the sample's concordia age and the $^{206}\text{Pb}/^{238}\text{U}$ weighted average age. For method 1, the relative deviations of concordia ages and $^{206}\text{Pb}/^{238}\text{U}$ weighted average ages for each sample compared to TIMS ages are less than 0.5%, while for method 2, these figures are less than 1.0% and 0.7%, respectively.

(2) Quantitative results of trace elements

The results of trace element analysis in zircon samples are shown in Table 3. The detection limits for REE range between 11ng/g and 73ng/g, with the majority being below 20ng/g. Among these, the detection limits for La and Pr are 20ng/g and 13ng/g, respectively. Ti has the highest detection limit, reaching up to 302ng/g, while Pb, Th, and U have the lowest detection limits at 15ng/g, 4ng/g, and 2ng/g, respectively.

Si and Zr were employed as internal standard elements for quantitative analysis. All quantitative results of zircon samples using Si as the internal standard element show slightly higher values overall than those calculated

using Zr as the internal standard element (Fig.2b). For the 91500 and SA01 samples, the analysis results using Si as the internal standard exhibit relative errors of less than 10% compared to the recommended values in literature [35] and [48]. However, when using Zr as the internal standard, the relative errors range between 10% and 20%. Furthermore, due to significant differences in Zr content between zircon and the selected standard samples, prolonged flushing is required after zircon analysis to decrease the background Zr levels in the instrument under conditions of high aerosol diffusion space. This prolonged flushing might impact the accuracy of Zr detection in the standard samples.

参考文献

- [1] Engi M. Petrochronology based on REE-minerals: Monazite, allanite, xenotime, apatite[J]. *Reviews in Mineralogy and Geochemistry*, 2017, 83(1): 365–418.
- [2] 赵令浩, 詹秀春, 曾令森, 等. 磷灰石 LA-ICP-MS U-Pb 定年直接校准方法研究[J]. 岩矿测试, 2022, 41(5): 744–753.
Zhao L H, Zhan X C, Zeng L S, et al. Direct calibration method for LA-HR-ICP-MS apatite U-Pb dating[J]. *Rock and Mineral Analysis*, 2022, 41(5): 744–753.
- [3] Chew D M, Spikings R A. Apatite U-Pb thermochronology: A review[J]. *Minerals*, 2021, 11(10): 1095–1116.
- [4] 赵令浩, 曾令森, 詹秀春, 等. 楠石 LA-SF-ICP-MS U-Pb 定年及对结晶和封闭温度的指示[J]. *岩石学报*, 2020, 36(10): 2983–2994.
Zhao L H, Zeng L S, Zhan X C, et al. *In situ* U-Pb dating of titanite by LA-SF-ICP-MS and insights into titanite crystallization and closure temperature[J]. *Acta Petrologica Sinica*, 2020, 36(10): 2983–2994.
- [5] Luo T, Zhao H, Zhang W, et al. Non-matrix-matched analysis of U-Th-Pb geochronology of bastnäsite by laser ablation inductively coupled plasma mass spectrometry[J]. *Science China: Earth Sciences*, 2021, 64(4): 667–676.
- [6] Hoskin P W O, Schaltegger U. The composition of zircon and igneous and metamorphic petrogenesis[J]. *Reviews in Mineralogy and Geochemistry*, 2003, 53(1): 27–62.
- [7] Toscano M, Pascual E, Nesbitt R W, et al. Geochemical discrimination of hydrothermal and igneous zircon in the Iberian Pyrite Belt, Spain[J]. *Ore Geology Reviews*, 2014, 56: 301–311.
- [8] Rubatto D. Zircon trace element geochemistry: Partitioning with garnet and the link between U-Pb ages and metamorphism[J]. *Chemical Geology*, 2002, 184(1–2): 123–138.
- [9] Pyle J, Spear F. Yttrium zoning in garnet: Coupling of major and accessory phases during metamorphic reactions[J]. *American Mineralogist*, 2003, 88(4): 708.
- [10] Henrichs I A, Chew D M, O’Sullivan G J, et al. Trace element (Mn-Sr-Y-Th-REE) and U-Pb isotope systematics of metapelitic apatite during progressive greenschist- to amphibolite-facies barrovian metamorphism[J]. *Geochemistry, Geophysics, Geosystems*, 2019, 20(8): 4103–4129.
- [11] O’Sullivan G, Chew D, Kenny G, et al. The trace element composition of apatite and its application to detrital provenance studies[J]. *Earth-Science Reviews*, 2020, 201: 103044.
- [12] Watson E B, Harrison T M. Zircon thermometer reveals minimum melting conditions on earliest Earth[J]. *Science*, 2005, 308(5723): 841–844.
- [13] Hayden L A, Watson E B, Wark D A. A thermobarometer for sphene (titanite)[J]. *Contributions to Mineralogy and Petrology*, 2008, 155(4): 529–540.
- [14] Ballard J R, Palin J M, Campbell I H. Relative oxidation states of magmas inferred from Ce(IV)/Ce(III) in zircon: Application to porphyry copper deposits of Northern Chile[J]. *Contributions to Mineralogy and Petrology*, 2002, 144(3): 347–364.
- [15] Zeng L, Asimow P D, Saleeby J B. Coupling of anatetic reactions and dissolution of accessory phases and the Sr and Nd isotope systematics of anatetic melts from a metasedimentary source[J]. *Geochimica et Cosmochimica Acta*, 2005, 69(14): 3671–3682.
- [16] Zeng L, Gao L E, Zhao L, et al. The role of titanite in shaping the geochemistry of amphibolite-derived melts[J]. *Lithos*, 2021, 402–403: 106312.
- [17] 赵令浩, 曾令森, 胡明月, 等. 金红石-榍石转变过程中元素地球化学行为——以雅鲁藏布江缝合带角闪岩为例[J]. 岩石学报, 2017, 33(8): 2494–2508.
Zhao L H, Zeng L S, Hu M Y, et al. Rutile to titanite transformation in amphibolite and its geochemical consequences: A case study of the amphibolite from Yarlung Tsangpo suture zone[J]. *Acta Petrologica Sinica*, 2017, 33(8): 2494–2508.
- [18] 赵令浩, 曾令森, 高利娥, 等. 变基性岩部分熔融过程

- 中榍石的微量元素效应:以南迦巴瓦混合岩为例[J].
岩石学报, 2020, 36(9): 2714–2728.
- Zhao L H, Zeng L S, Gao L E, et al. Role of titanite in the redistribution of key trace elements during partial melting of meta-mafic rocks: An example from Namche Barwa migmatite[J]. *Acta Petrologica Sinica*, 2020, 36(9): 2714–2728.
- [19] Zhao L, Zeng L, Gao L, et al. Rutile to titanite transformation in eclogites and its geochemical consequences: An example from the Sumdo Eclogite, Tibet[J]. *Acta Geologica Sinica-English Edition*, 2023, 97(1): 122–133.
- [20] Engi M, Lanari P, Kohn M. Significant ages—An introduction to petrochronology[J]. *Reviews in Mineralogy and Geochemistry*, 2017, 83(1): 1–12.
- [21] Wei Q D, Yang M, Romer R L, et al. *In situ* U-Pb geochronology of vesuvianite by LA-SF-ICP-MS[J]. *Journal of Analytical Atomic Spectrometry*, 2022, 37(1): 69–81.
- [22] Seman S, Stockli D F, McLean N M. U-Pb geochronology of grossular-andradite garnet[J]. *Chemical Geology*, 2017, 460: 106–116.
- [23] Woodhead J, Petrus J. Exploring the advantages and limitations of *in situ* U-Pb carbonate geochronology using speleothems[J]. *Geochronology*, 2019, 1: 69–84.
- [24] Li D, Tan C, Miao F, et al. Initiation of Zn-Pb mineralization in the Pingbao Pb-Zn skarn district, South China: Constraints from U-Pb dating of grossular-rich garnet[J]. *Ore Geology Reviews*, 2019, 107: 587–599.
- [25] Yang Y H, Wu F Y, Yang J H, et al. U-Pb age determination of schorlomite garnet by laser ablation inductively coupled plasma mass spectrometry[J]. *Journal of Analytical Atomic Spectrometry*, 2018, 33(2): 231–239.
- [26] Kylander-Clark A R C, Hacker B R, Cottle J M. Laser-ablation split-stream ICP petrochronology[J]. *Chemical Geology*, 2013, 345: 99–112.
- [27] Hattendorf B, Latkoczy C, Günther D. Peer reviewed: Laser ablation-ICPMS[J]. *Analytical Chemistry*, 2003, 75(15): 341A–347A.
- [28] Kooijman E, Berndt J, Mezger K. U-Pb dating of zircon by laser ablation ICP-MS: Recent improvements and new insights[J]. *European Journal of Mineralogy*, 2012, 24: 5–21.
- [29] Wu S, Yang M, Yang Y, et al. Improved *in situ* zircon U-Pb dating at high spatial resolution (5–16 μm) by laser ablation-single collector-sector field-ICP-MS using jet sample and X skimmer cones[J]. *International Journal of Mass Spectrometry*, 2020, 456: 116394.
- [30] Roberts N M W, Rasbury E T, Parrish R R, et al. A calcite reference material for LA-ICP-MS U-Pb geochronology[J]. *Geochemistry, Geophysics, Geosystems*, 2017, 18(7): 2807–2814.
- [31] Latkoczy C, Günther D. Enhanced sensitivity in inductively coupled plasma sector field mass spectrometry for direct solid analysis using laser ablation (LA-ICP-SFMS)[J]. *Journal of Analytical Atomic Spectrometry*, 2002, 17(10): 1264–1270.
- [32] Wiedenbeck M, Allé P, Corfu F, et al. Three natural zircon standards for U-Th-Pb, Lu-Hf, trace element and REE analyses[J]. *Geostandards Newsletter*, 1995, 19(1): 1–23.
- [33] Jackson S E, Pearson N J, Griffin W L, et al. The application of laser ablation-inductively coupled plasma-mass spectrometry to *in situ* U-Pb zircon geochronology[J]. *Chemical Geology*, 2004, 211: 47–69.
- [34] Hu Z, Li X H, Luo T, et al. Tanz zircon megacrysts: A new zircon reference material for the microbeam determination of U-Pb ages and Zr-O isotopes[J]. *Journal of Analytical Atomic Spectrometry*, 2021, 36(12): 2715–2734.
- [35] Huang C, Wang H, Yang J H, et al. SA01—A proposed zircon reference material for microbeam U-Pb age and Hf-O isotopic determination[J]. *Geostandards and Geoanalytical Research*, 2020, 44(1): 103–123.
- [36] Black L P, Kamo S L, Allen C M, et al. TEMORA 1: A new zircon standard for Phanerozoic U-Pb geochronology[J]. *Chemical Geology*, 2003, 200(1): 155–170.
- [37] Sláma J, Košler J, Condon D J, et al. Plešovice zircon—A new natural reference material for U-Pb and Hf isotopic microanalysis[J]. *Chemical Geology*, 2008, 249(1-2): 1–35.
- [38] 李献华, 唐国强, 龚冰, 等. Qinghu(清湖)锆石:一个新的U-Pb年龄和O, Hf同位素微区分析工作标样[J]. *科学通报*, 2013, 58(20): 1954–1961.
Li X H, Tang G Q, Gong B, et al. Qinghu zircon: A working reference for microbeam analysis of U-Pb age and Hf and O isotopes[J]. *Chinese Science Bulletin*, 2013, 58(20): 1954–1961.
- [39] Horn I, Günther D. The influence of ablation carrier gasses Ar, He and Ne on the particle size distribution and transport efficiencies of laser ablation-induced aerosols: Implications for LA-ICP-MS[J]. *Applied Surface Science*, 2003, 207(1-4): 144–157.
- [40] Hu Z, Gao S, Liu Y, et al. Signal enhancement in laser

- ablation ICP-MS by addition of nitrogen in the central channel gas[J]. *Journal of Analytical Atomic Spectrometry*, 2008, 23(8): 1093–1101.
- [41] Griffin W, Powell W, Pearson N J, et al. GLITTER: Data reduction software for laser ablation ICP-MS[M]//Sylvester P. Laser ablation-ICP-MS in the Earth sciences. Mineralogical Association of Canada, 2008: 204-207.
- [42] Ludwig K R. User's manual for Isoplot 3.6: A geochronological toolkit for Microsoft excel[M]. Berkeley Geochronology Center, 2003.
- [43] 李献华, 柳小明, 刘勇胜, 等. LA-ICPMS 钨石 U-Pb 定年的准确度: 多实验室对比分析[J]. 中国科学: 地球科学, 2015, 45(9): 1294-1303.
Li X H, Liu X M, Liu Y S, et al. Accuracy of LA-ICPMS zircon U-Pb age determination: An inter-laboratory comparison [J]. *Science China: Earth Sciences*, 2015, 58: 1722-1730.
- [44] Horstwood M, Košler J, Gehrels G, et al. Community-derived standards for LA-ICP-MS U-(Th)-Pb geochronology—Uncertainty propagation, age interpretation and data reporting[J]. *Geostandards and Geoanalytical Research*, 2016, 40(3): 311–332.
- [45] Fisher C, Longerich H, Jackson S, et al. Data acquisition and calculation of U-Pb isotopic analyses using laser ablation (single collector) inductively coupled plasma mass spectrometry[J]. *Journal of Analytical Atomic Spectrometry*, 2010, 25: 1905–1920.
- [46] Schoene B, Condon D, Morgan L, et al. Precision and accuracy in geochronology[J]. *ELEMENTA*, 2013, 9: 19–24.
- [47] Liu Y, Hu Z, Zong K, et al. Reappraisal and refinement of zircon U-Pb isotope and trace element analyses by LA-ICP-MS[J]. *Chinese Science Bulletin*, 2010, 55(15): 1535–1546.
- [48] Wiedenbeck M, Hanchar J M, Peck W H, et al. Further characterisation of the 91500 zircon crystal[J]. *Geostandards and Geoanalytical Research*, 2004, 28(1): 9–39.
- [49] Zhao K D, Jiang S Y, Ling H F, et al. Reliability of LA-ICP-MS U-Pb dating of zircons with high U concentrations: A case study from the U-bearing Douzhashan granite in South China[J]. *Chemical Geology*, 2014, 389: 110–121.
- [50] Marillo-Sialer E, Woodhead J, Hanchar J M, et al. An investigation of the laser-induced zircon ‘matrix effect’[J]. *Chemical Geology*, 2016, 438: 11–24.